Turk J Phys
25 (2001) , 455 – 466.

Production and Structure of Rapidly Solidified Al-Si Alloys

Orhan UZUN
Department of Physics, Gaziosmanpaşa University, 60110 Tokat-TURKEY
Tuncay KARAASLAN
Department of Physics, Erciyes University, 38039 Kayseri-TURKEY
Mustafa KESKİN
Department of Physics, Erciyes University, 38039 Kayseri-TURKEY

Received 10.10.2000

Abstract

Al-Si alloys with compositions 8, 12, 16wt% Si were manufactured by chill casting and melt-spinning (MS) methods. The resulting ribbon samples have been characterized by optical and scanning electron microscopy (SEM) and X-ray diffractometry and compared with their ingot counterparts. Microstructural examinations revealed that microstructures of the melt-spun ribbons were quite fine compared to their ingot counterparts. Both XRD analyses and microstructural examinations indicated that the solubility of Si in α-Al phase was nearly complete.

1. Introduction

In 1960, Duwez and his co-workers developed a novel technique to extend solid solubility [1] and to produce metastable crystalline [2] or amorphous [3] solid phase in some simple binary eutectic alloy systems. In fact, Russian researcher Salli was the first to apply a method similar to one above in 1958 [4]. Both researchers employed a "gun technique" in which a small droplet of molten metal impacted on a chill surface with high velocity, resulting in a non-uniform "splat" of solidified material. The cooling rates for this process were estimated within the range of 10^5 to 10^6 Ks^{-1}, much faster than the conventional solidification rates which are 10^2 Ks^{-1} or less [5, 6]. Since the introduction of rapid quenching of metallic melts by Duwez, a great variety of techniques have been developed to obtain alloys produced by rapid solidification. Although, the effect of rapid solidification vary widely from system to system, the major effects are: **(i)** decreased in grain size, **(ii)** increased in chemical homogeneity, **(iii)** extension of solid solubility limits, **(iv)** creation of metastable crystalline phases, and **(v)** formation of metallic glasses [7, 8].

The density of silicon (Si) is 2.3 gr/cm^3 and of aluminium (Al) is 2.7 gr/cm^3 so that Si is one of the few elements which may be added to Al without loss of weight advantage. Additionally, the relatively low coefficient of thermal expansion, high wear resistance and fluidity that are characteristic of Al-Si alloys have received considerable interest in this alloy family as candidate materials for automotive and aerospace applications [9, 10]. Therefore, Al-Si alloys are sought in a large number of applications in the automobile industries, e.g. for pistons, cylinder blocks and liners [6, 11]. However, under the conventional solidification conditions, the Si phase in cast Al-Si alloys often exhibit a coarse microstructure that leads to poor mechanical properties [6, 10].

Recent results have demonstrated that rapid solidification processes may substantially modify the morphology of the Si phase as compared to those found in conventionally processed materials [6, 12-14]. Therefore, various rapid solidification techniques have been applied to wide range of composition of Al-Si alloys. Among them splat quenching [15, 16], atomization [17-19], and melt spinning [11, 19-23] resulted in an increase in the solid solubility of Si in α-Al without forming any intermetallic compounds. While some of these attempts [15-18] focused on microstructural characterization of rapidly solidified Al-Si alloys, others [19-23] concentrated on finding optimal value for determining the retained-Si amount in α-Al by X-ray diffraction methods, depending on lattice parameter change of Al solid solution. However, these studies have suggested many different values, ranging from 3.7x10^{-5} nm to 1.23x10^{-3} nm, for each increasing 1at% retained-Si amount in α-Al.

In this work, the Al-Si system has been chosen essentially due to its technological importance. Therefore, the present study focused on structural characterization of rapidly solidified Al-Si alloys comparatively with their conventionally produced (ingot) counterparts. Although rapid solidification may increase the equilibrium solid solubility of Si in α-Al, how the amount of retained-Si in Al solid solution can be determined is still controversial. Hence, the main purpose of the present study was to determine the retained Si amount in the α-Al phase in detail.

2. Melt-Spinning Processing

A large number of devices designed for producing rapid solidification material have been reported over the last three decades and these can be classified in many different ways. Jones [24] classifies them into three categories: **(i)** spray methods, **(ii)** surface methods, and **(iii)** chill methods.

Spray methods involve with the production of a liquid metal spray, which is later to be rapidly solidified. The various devices in spray methods differ in two aspects as: Those ones used for production of the liquid spray and those for quenching. The spray methods include spray atomization and deposition, and the gun technique.

The most significant characteristic of the weld method is that both melting and solidification occur in situ at the chill surface, which may itself be partially melted in the processes [24].

The principle involved with chill methods is the production of a thin section of liquid

metal that is cooled by a larger chill block. Among these types of methods the melt spinning is the most widely used one because of its relatively high cooling rates up to 10^6 Ks^{-1}, enabling production of the metastable crystalline or amorphous continuous strips. In addition to that, the high practicality of the technique favours high volume industrial manufacturing [25, 26]. In fact, the development of this technique has been primarily responsible for the accelerated progress of rapid solidification technology since the seventies.

The name of the melt-spinning process derives from its involvement with the extrusion of molten metal in a way which is akin to that used to manufacture synthetic textile fibres. The melt-spinning can be carried out either by extruding a liquid stream into a cooling medium, called the free flight melt-spinning (FFMS), or by allowing a molten jet to impinge on a rotating chill block, called chill block melt spinning (CBMS). The former method is well known to polymer technologists while the later dates back to 1908 and often used to provide rapidly solidified materials. In the present work, we also used the CBMS technique to produce melt-spun ribbons of Al-Si alloys.

3. Experimental

3.1. Specimen Preparation

The chill block melt-spinning device is schematically shown in Fig. 1. It basically consists of two parts: (i) the melting system and (ii) the rotating disc. The melting system consists of a fused silica tube 65 mm in diameter with complete openings at both ends. A close-fitting graphite crucible, with one end open the other restricted with a nozzle 2 mm in diameter, was placed into a fused silica tube. The graphite crucible is used to both heat the aluminum alloy and to hold the resulting melt. The fused silica tube was capped with a gas tight cap having an inlet in the center to let argon gas in. The rotating disc, 22 cm in diameter, was machined from a brass block. Temperature was measured by placing a cromel-alumel thermocouple at the central region of crucible wall.

Firstly, Al-Si alloys with nominal compositions of 8, 12, 16wt% Si were manufactured in ingot manner by melting 99.9% pure Al and 99.995% Si metals in a graphite crucible under vacuum. After that, these ingot materials were cut into pieces from which melt-spun ribbons will be produced by the Melt Spinning (MS) system. Secondly, these sectioned ingot materials were re-melted in a graphite crucible and spun into ribbons in the MS system. The molten alloy with an 850 °C was ejected from the crucible under an argon pressure of approximately $9{,}807.10^6$ Pa onto the brass wheel rotating at a surface velocity of 40 ms^{-1}. Thus, the rapidly solidified ribbons were produced ranging from 15 μm to 150 μm in thickness, from 1 mm to 4 mm in width and from 5 cm to 300 cm in length. As mentioned above, we can not give certain values for the average thickness, width and length. But the samples with the closest values for width, length and thickness were chosen to obtain the greatest possible uniformity.

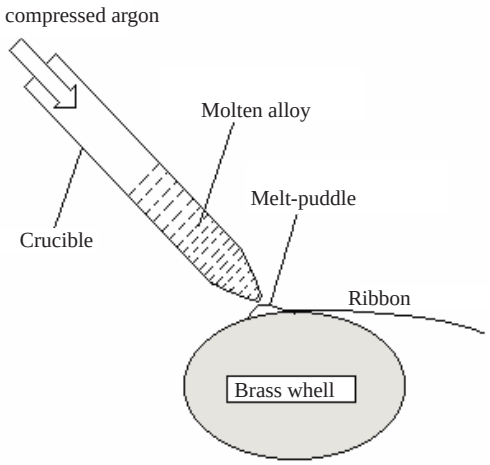

Figure 1. Schematic of melt-spinning process.

3.2. Metallography

Micro structural examinations of both ingot and ribbon samples were carried out with an Olympus BH2 optical microscope (OM) and the JEOL JSM 5400 scanning electron microscope (SEM). Wheel and air sides of ribbons and ingot samples were examined after mechanical polishing and etching in a Keller-Wilcox reagent. After the specimens were coated with a gold layer to enhance contrast, SEM micrographs were usually taken at an accelerating voltage of 20 kV.

3.3. X-ray diffraction

For X-ray diffraction analyses, each ingot and ribbon were produced then examined without application of any treatment. X-ray diffraction studies for phase analyses and the lattice parameter measurements were performed using a Rigaku D/max-IIIC Diffractometer. X-ray diffraction patterns were obtained utilizing CuK_α radiation with a wavelength λ of 1.5406 Å. For phase identification, measurements were scanned for a wide range of diffraction angles (2θ) ranging from 20 to 100 degrees with a scanning rate of 5 deg/min. The lattice parameters were determined from the {422} index planes reflections of the aluminium-based solid solution. To enhance the accuracy of X-ray measurements for the lattice parameter of α-Al, both scanning interval and scanning rate were decreased to 0.004 degree and 0.2 deg/min, respectively.

4. Results and Discussion

Microstructural analyses were conducted by optical and scanning electron microscopy. The microstructures of ingot samples, known as conventionally cast alloys, are given in

Figs. 2 and 3. Optical micrographs of ingot Al-8wt% Si alloy are given in Fig. 2 a-b. Both micrographs, showed similar microstructures with a nonuniform distribution of needle-like Si particles in the matrix of α-Al. The micrographs of Al-12wt% Si alloy, given in Fig. 2 c-d, also showed similar microstructure as Al-8wt% Si, except with increasing Si concentration. Similar results have been reported elsewhere [27-29]. Al-16wt% Si alloy exhibits not only needle-like eutectic Si phase but also large faceted massive primary Si crystals that signify a hypereutectic microstructure (Fig. 2 e-f). When we consider the equilibrium phase diagram of Al-Si alloy, the above results would be expected.

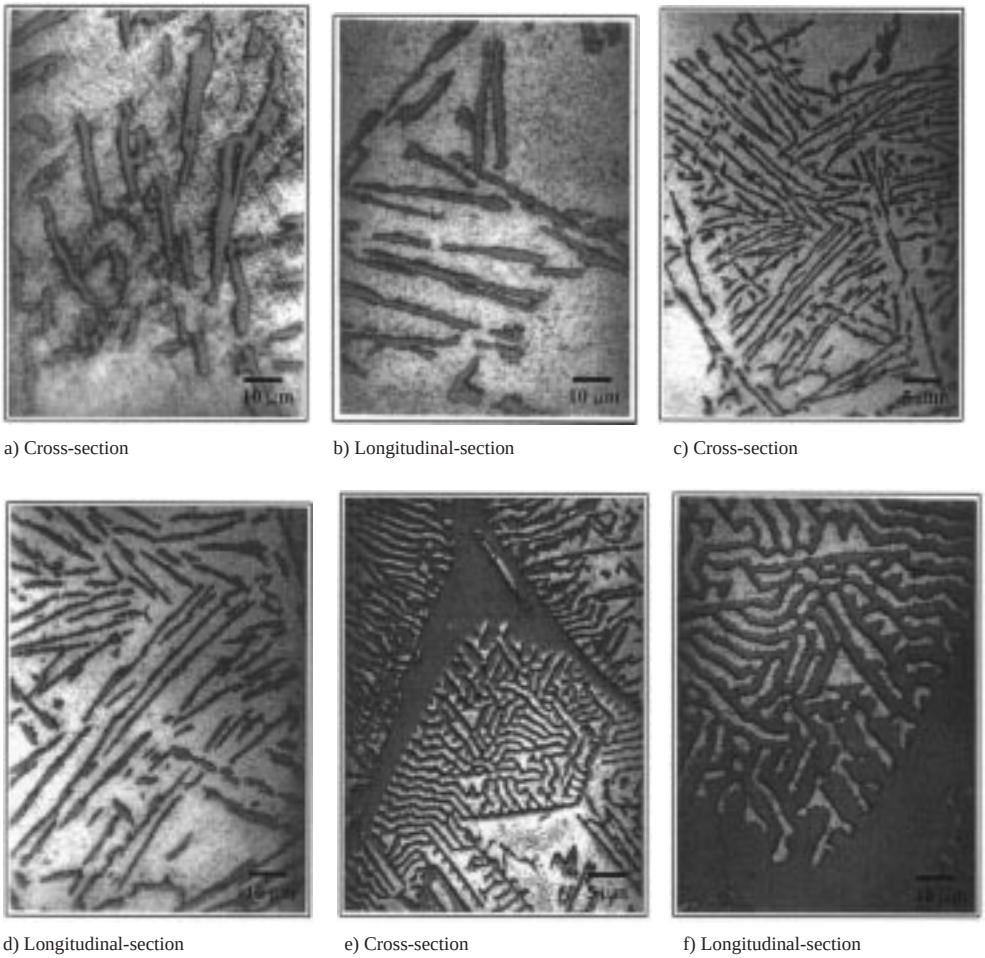

Figure 2. Optic micrographs of ingot (a, b) Al-8wt% Si (c, d) Al-12wt% Si (e, f) Al-16wt% Si alloys.

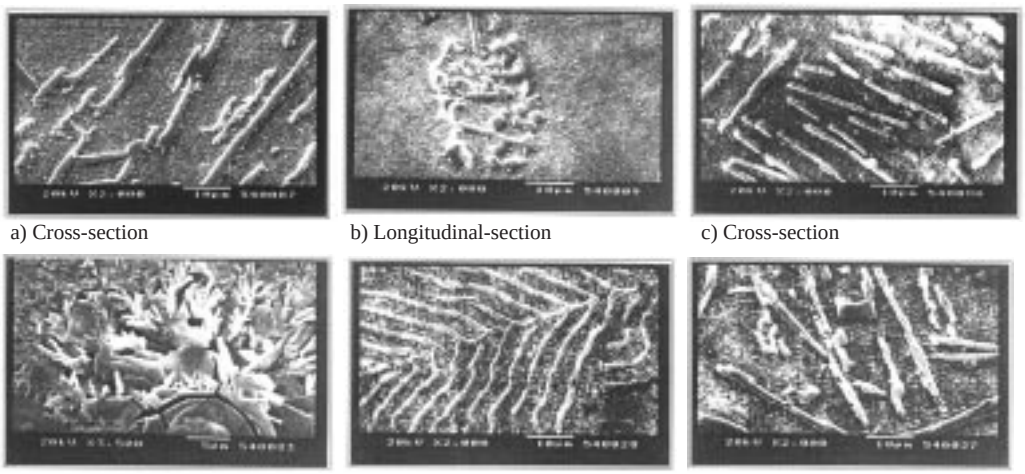

a) Cross-section b) Longitudinal-section c) Cross-section

d) Longitudinal-section e) Cross-section f) Longitudinal-section

Figure 3. SEM micrographs of ingot (a, b) Al-8wt% Si (c, d) Al-12wt% Si (e, f) Al-16wt% Si alloys.

SEM micrographs of the same Al-8, 12 and 16wt% Si ingot alloys are shown in Fig. 3 a-e. Similarly, those micrographs, given in Fig. 3 a-d, also showed nonuniform distribution of needle-like Si phase in the α-Al matrix for both 8 and 12wt% Si composition, while the Al-16wt% Si micrographs, given in Fig. 3 e-f, exhibit a hypereutectic microstructure.

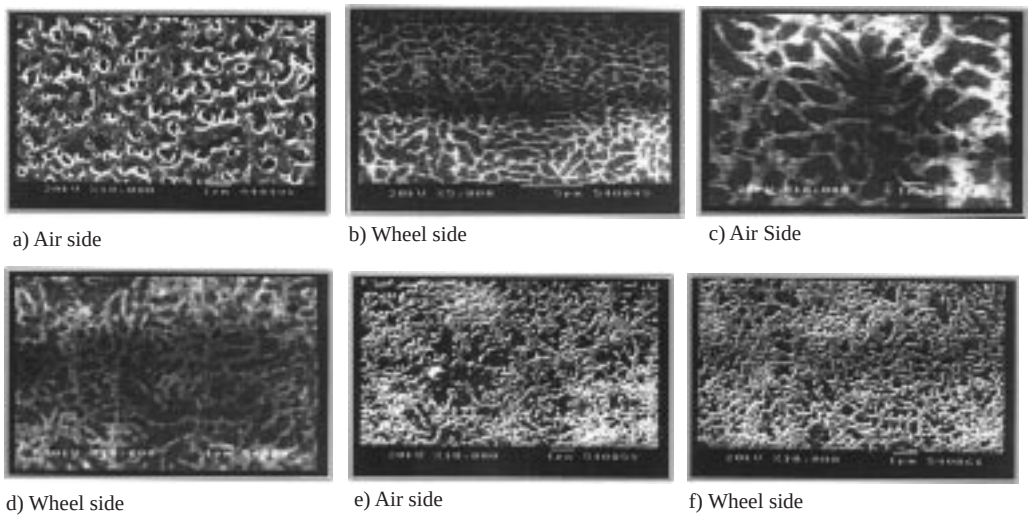

a) Air side b) Wheel side c) Air Side

d) Wheel side e) Air side f) Wheel side

Figure 4. SEM micrographs of melt-spun (a, b) Al-8wt% Si (c, d) Al-12wt% Si (e, f) Al-16wt% Si alloys.

The SEM analyses of the as-quenched ribbons were carried out on both surfaces to determine the cooling effect of the substrate. When we examine the air and wheel sides of ribbons, in Fig. 4, we notice that the air sides generally show a fine branched dendritic microstructure, while wheel sides commonly appear to possess a cellular microstructure for all melt-spun Al-8, 12, 16 wt% Si alloys. The cellular structure of ribbon containing 16wt% Si showed a slight difference from those of other samples, indicating the presence of a high Si ratio.

Micro structural examinations revealed that the structure of the specimens prepared by the melt-spinning method were quite different from those of ingot specimens. None of the primary Si crystal was observed in the SEM analysis of melt-spun ribbons in contrast to that of ingot counterparts. This result has revealed that, under the equilibrium conditions, a hypereutectic Al-16wt% Si alloy can have a hypoeutectic structure due to the exposure of undercooling through rapid quenching. This effect has been previously identified in eutectic metal systems [19]. Depending on the fastest growing phase at a given undercooling condition, a structure which consists of both primary and eutectic phases or only the later develops. In the aluminium-silicon system, the primary aluminium rich phase grows dendritically, whereas the silicon rich phase grows in a facetted manner. Comparing with dendritical phase, the faceted grows slower at undercooling. Previously, Jacobson and McKittrick [30] reported that relatively low undercooling application on an alloy of a given composition causes dendritical growth in which one of the phases grows rapidly and the other phase solidifies between dendrites while higher undercooling leads to cellular growth. Based on the above statements, we conclude that the difference between microstructures of both sides resulted from different cooling rates. That was expected due to the fact that solidification starts at the wheel side. Additionally, the lack of any observation of Si crystal is a result of suppression of silicon nucleation.

XRD patterns for all ingots and ribbons, illustrated in Figs. 5-7, show similarity in which all the possible α-Al and Si phase reflections are expectedly present. Those patterns for quenched ribbons, shown in the same figures with those of ingot specimens, also exhibited all the possible reflections of Al-solid solution, however, only very weak and broad reflections of Si were recognized. In contrast to the ingot case, the lack of Si reflections for quenched ribbons in the XRD analysis revealed that a substantial amount of Si has been retained in the solid solution. To determine the amount of retained-Si upon rapid quenching, the lattice parameter of α-Al phase was determined using Bragg's formula for both ingot and as-quenched ribbons. The lattice parameters for all Si contents are given in Table 1.

In theory, the lattice parameter of α-Al phase decreases with increasing Si content in the solid solution [11]. The quantity of decrease has been detected via the closest distance of approach of the constitutional atoms [11]. The amount of decrease in the lattice parameters for the 8, 12, 16wt% Si contents were determined as $\Delta a_1 = 6.4 \times 10^{-4}$ nm, $\Delta a_2 = 8.3 \times 10^{-4}$ nm, and $\Delta a_3 = 9.3 \times 10^{-4}$ nm, respectively, as calculated in earlier studies [19-21]. The variability in the α-Al lattice parameters resulted from extension of Si solid solubility in Al-Si alloys has earlier been reported by several researchers [19-23].

Table. Lattice parameters and lattice parameter changes of α-Al for each melt-spun and ingot alloys

Sample	Method of Alloy Production	Lattice Parameter (a; nm±0.0005)	Lattice Parameter Change (Δa; nm±0.0005)
Al-8wt% Si	Ingot	0.40490	$6.4\text{x}10^{-4}$
	Melt-Spun	0.40426	
Al-12wt% Si	Ingot	0.40500	$8.3\text{x}10^{-4}$
	Melt-Spun	0.40417	
Al-16wt% Si	Ingot	0.40505	$9.3\text{x}10^{-4}$
	Melt-Spun	0.40412	

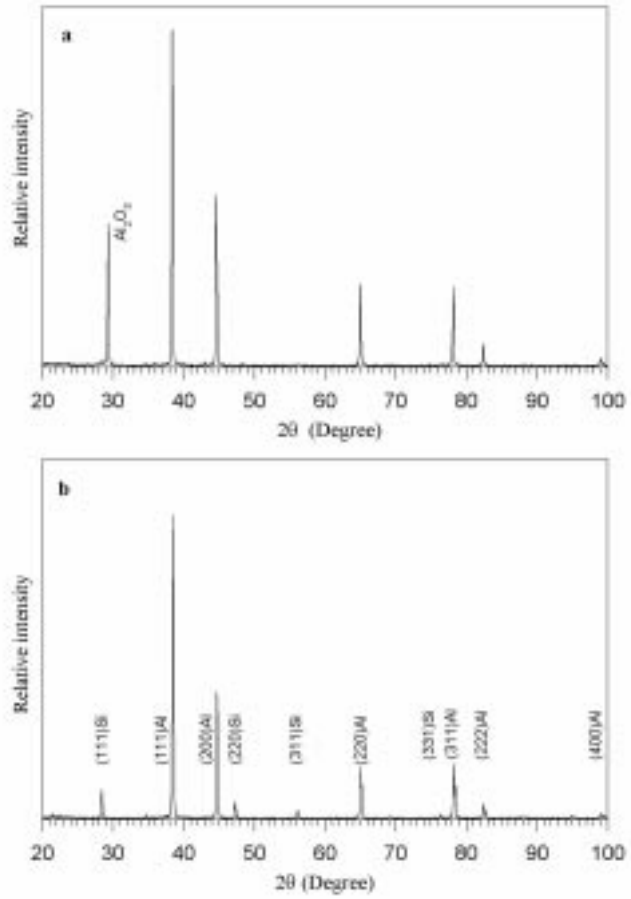

Figure 5. The XRD patterns of Al-8wt% Si, a) Ribbons, b) Ingot alloys.

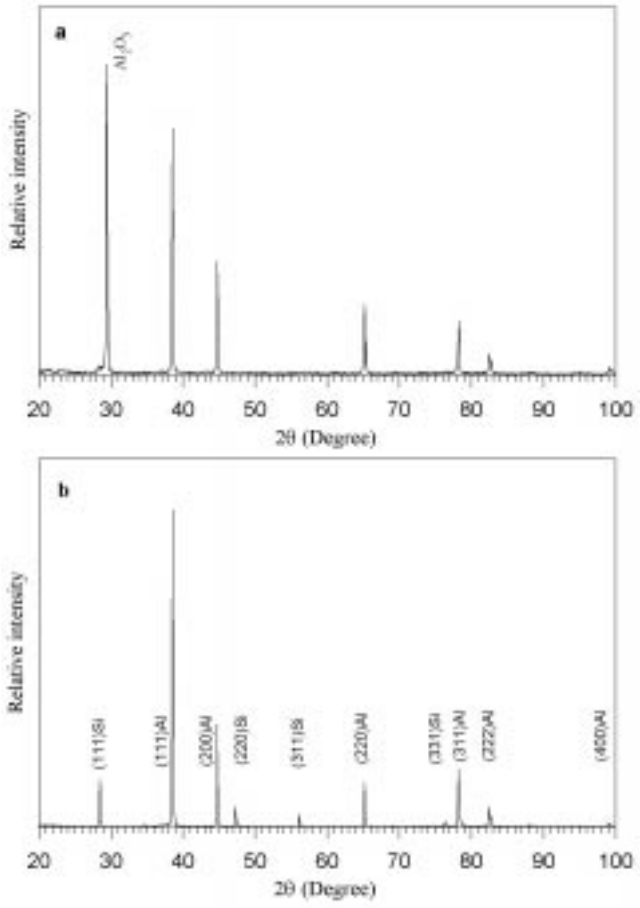

Figure 6. The XRD patterns of Al-12wt% Si, a) Ribbons, b) Ingot alloys.

These values, for change in lattice parameters (Δ_s), ranging from $3.7\text{x}10^{-5}$ nm to $1.23\text{x}10^{-3}$ nm, were reported, and defining each increasing 1at% retained-Si in α-Al solid solution. The amounts of retained-Si in α-Al calculated from both of the lowest and highest Δ_s values would be quite different. For instance, while the highest value taken as the change in lattice parameter, the retained-Si amount would be 1% , that responds 33% retained-Si based on the assumption in which the lowest value accepted as the change in lattice parameter.

Contrary to ingot counterparts, XRD analyses of melt-spun Al-8, 12, 16wt% Si alloys did not exhibit any strong and sharp Si reflection (Figs. 5-7). There is only a very weak and broad (111) reflection. Therefore, we may say that the all added Si amount were nearly solved in α-Al for each melt-spun Al-Si alloys. However, because of the very weak and broad Si reflections in the melt-spun ribbons, a certain Si amount could be lost in the

background without being observed. In our XRD analyses of all melt-spun alloys, none of the possible reflections from the (220) index planes with 55% relative intensity were observed. Similarly, the possible reflections with the lower relative intensities from the other index planes [(311), (400), (331), (422)] were not observed. Hence, we can conclude that at least 55% of the added Si amounts have been solved in α-Al for all melt-spun alloys. These values are 4.4wt% for 8wt% Si; 6.6wt% Si for 12wt% Si; 8.8wt% Si for 16wt% Si contents. Thus, we can say that the application of melt-spinning method in producing melt-spun alloys significantly enhances the equilibrium solid solubility limit of Si in α-Al, which was reported as 0.02wt% Si at room temperature [10, 31].

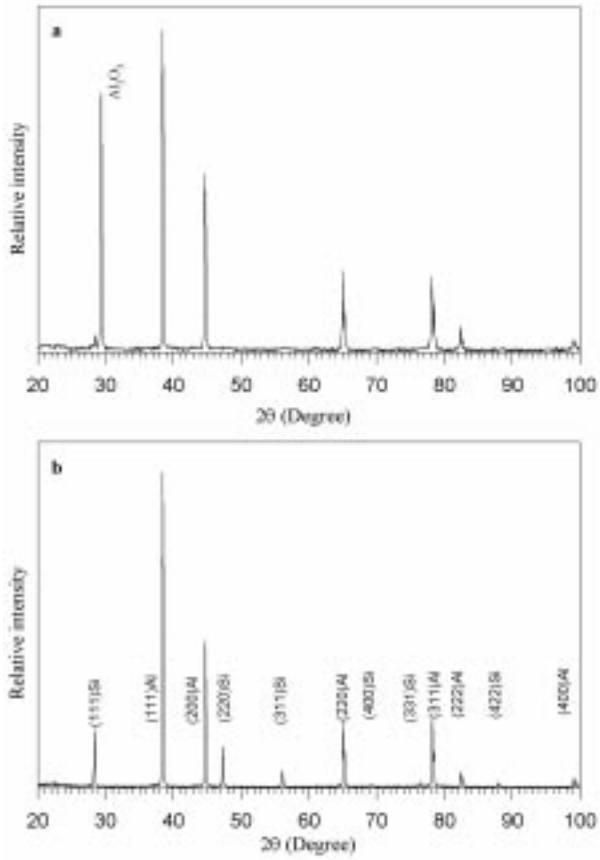

Figure 7. The XRD patterns of Al-16wt% Si, a) Ribbons, b) Ingot alloys.

On the other hand, XRD analyses show that each melt-spun ribbon had one sharp and high Al_2O_3 reflection contrary to ingot counterparts possessing none. However, none of other possible Al_2O_3 reflections was detected. This remarkable observation resulted

from the parallel orientation of oxide film to the ribbon surface without presence of any intermetallic phase. The lack of any intermetallic phase in microstructural examinations supports the suggestion stated above. The oxide film on the ribbon surface resulted because vacuum was not used during the MS.

5. Conclusions

1. Different cooling rates result in different microstructures on both air and wheel sides of ribbons.
2. The suppression of silicon nucleation prevents the formation of Si crystal on the Al-based matrix.
3. Both XRD and microstructural analyses show that the MS extends the solid solubility of Si in α-Al of ingot alloys.
4. The use of relative intensities of the diffraction lines gives more accurate values for retained-Si amount in α-Al compared with the use of the lattice parameters change.

Acknowledgements

We would like to express our gratitude to TÜBİTAK for their financial support (Grant No: TBAG-AY/75). The financial supports from Research Foundation of GOU (Grant No: 95-31, 96-20 and 00-08) and Erciyes University (Grant No: 96-051-1) are also gratefully acknowledged.

References

[1] P. Duwez, R. H. Willens and W. Klement, *J. Appl. Phys.*, **31** (1960) 1136.

[2] P. Duwez, R. H. Willens and W. Klement, *J. Appl. Phys.*, **31** (1960) 1500.

[3] W. Klement, R. H. Willens and P. Duwez, *Nature*, **187** (1960) 869.

[4] I. V. Salli, *Liteinoe Proizvodstvo*, **7** (1958) 22.

[5] T. R. Anantharaman and C. Suryanarayana, *Rapidly solidified metals*, (Trans Tech Pub., Switzerland 1987) p.5.

[6] S. Das, A. H. Yegnesvaran and P. K. Rohatgi, *J. Mat. Sci.*, **22** (1987) 3173.

[7] H. Jones, *Mat. Sci. Eng.*, **A133** (1991) 33.

[8] B. Cantor, W. T. Kim, B. P. Bewley and A. G. Gillen, *J. Mat . Sci.*, **26** (1991) 1266.

[9] B. K. Prasad, *J. Mat. Sci.*, **10** (1991) 867.

[10] O. Uzun, Ph.D. Thesis, Department of Physics, Gazi University Institute of Science and Technology, Turkey, 1998.

[11] S. Su, X. Liang, A. Moran and E. J. Lavernia, *Int. J. Rap. Sol.*, **8** (1994) 161.

[12] N. Fat-Halla, *J. Mat . Sci.*, **22** (1987) 1013.

[13] M. Rooyen, N. M. Van Der Pers, Th. H. Keijser and E. J. Mittemeijer, *Mat. Sci. Eng.,* **96** (1987) 17.

[14] B. K. Yen, J. Mat . Sci., **32** (1997) 821.

[15] M. Itagaki, B. C. Giessen and N. J. Grant, *Trans. Quart. ASM.,* **61** (1968) 330.

[16] H. Matja, K. C. Russel, B. C. Giessen and N. J. Grant, *Metall. Trans.* **A, 6** (1975) 2249.

[17] I. Yamauchi, I. Ohnaka, S. Kawamoto and T. Fukusako, *Trans. Jap. Ins. Met.,* **27, 3** (1986) 187.

[18] S. J. Hong, T. S. Kim, W. T. Kim and B. S. Chun, *Mat. Sci. Eng.* **A226** (1997) 878.

[19] P. Todeshini, G. Champier and F. H. Samuel, *J. Mat. Sci.,* **27** (1992) 3551.

[20] S. K. Bose and R. Kumar, *J. Mat. Sci.*, **8** (1973) 1795.

[21] A. Bendijk, R. Delhez, L. Katgerman, Th. H. De Keijsher, E. J. Mittemeijer and N. M. Van Der Pers, *J. Mat. Sci.,* **15** (1986) 2803.

[22] M. Rooyen, N. M. Van Der Pers, Th. H. Keijser and E. J. Mittemeijer, *Mat. Sci. Eng.,* **96** (1987) 17.

[23] A. M. Bastawros and M. Z. Said, J. Mat. Sci., **28** (1993) 1143.

[24] H. Jones, *Mat. Sci. Eng.,* **65** (1984) 145

[25] R. W. Cahn, K. D. Laridjani, M. Greenholtz and R. Hill, *Mat. Sci . Eng.,* **23** (1976) 83.

[26] R. B. Pond, R. E. Maringer and C. E. Mobley, ASM seminar series, (1976) 20.

[27] F. Yılmaz and R. Elliott, *J. Mat.Sci.,* **24** (1989) 2065.

[28] N. Fat-Halla, *J. Mat. Sci.,* **24** (1989) 2488.

[29] D. R. Allen, M. Gremaud and J. H. Perepezko, *Mat. Sci. Eng.,* **A226** (1997) 173.

[30] L. A. Jacobson and J. McKittrick, *Mat. Sci. Eng.,* **R11**, **8** (1994) 355.

[31] T. B. Massalski, Binary alloys phase diagrams, (American Soc. for Met., Ohio 1986) p.165.